



 Cite this: *RSC Adv.*, 2021, 11, 38016

## Two-step preparation of Keggin-PW<sub>12</sub>@UIO-66 composite showing high-activity and long-life conversion of soybean oil into biodiesel

 Yuxin Zhang, Xinluo Song, Shicong Li, Bangyao Zhao, Liangliang Tong, Yuanrui Wang\* and Yafeng Li \*

A polyoxometalate acid can be encapsulated into a metal–organic framework to construct a novel kind of solid-acid catalyst. In this work, the two-step method—high-temperature preparation of Zr<sub>6</sub>O<sub>4</sub>(OH)<sub>4</sub>(CH<sub>3</sub>COO)<sub>12</sub> and low-temperature self-assembly—has been adopted to synthesize the PW<sub>12</sub>@UIO-66 composite (PW<sub>12</sub> = H<sub>3</sub>PW<sub>12</sub>O<sub>40</sub>; UIO-66 = Zr<sub>6</sub>O<sub>4</sub>(OH)<sub>4</sub>(OOC–C<sub>6</sub>H<sub>4</sub>–COO)<sub>12</sub>). The as-synthesized PW<sub>12</sub>@UIO-66 composite exhibits highly crystalline, good octahedron morphology, large specific surface area (1960 m<sup>2</sup> g<sup>−1</sup>) and high thermal stability (>500 °C), which clearly demonstrates the potential as a solid-acid catalyst. Additionally, the PW<sub>12</sub>@UIO-66 composite may be accomplished with 85% utilization of H<sub>3</sub>PW<sub>12</sub>O<sub>40</sub> and 95% yield through this synthetic procedure. The performances of the PW<sub>12</sub>@UIO-66 composite are investigated by catalyzing the simultaneous transesterification and esterification of soybean oil into biodiesel. Under the optimal conditions, the conversion of the soybean oil into biodiesel would exceed 90% over the as-synthesized PW<sub>12</sub>@UIO-66 composite. As the crucial indexes for industrial prospects, the recycling and life experiments were surveyed. After 10 times recycling and 4 weeks, the structure and performance of the PW<sub>12</sub>@UIO-66 composite remained unchanged and in the meantime the PW<sub>12</sub>@UIO-66 composite still maintained a high activity to convert soybean oil into biodiesel.

 Received 17th August 2021  
 Accepted 16th November 2021

DOI: 10.1039/d1ra06211e

[rsc.li/rsc-advances](http://rsc.li/rsc-advances)

### 1. Introduction

Acid-catalyzed chemical reactions have been featuring prominently in the chemical industry. Compared with mineral acids, a solid-acid catalyst has the advantages of environmental benignity, easy separation, non-corrosion and recycling *etc.*<sup>1–3</sup> However, the life of a solid-acid catalyst seriously restrains its industrial prospects. To design a novel solid-acid catalyst continuously is a challenging research field. Usually, a solid-acid catalyst can be fabricated by loading mineral acid on a carrier.<sup>4,5</sup> A simple way to prolong the life of a solid-acid catalyst is to strengthen the interaction between mineral acid and carrier.<sup>6</sup> Additionally, the encapsulation of mineral acid into channels or cages of the carrier microstructure is an alternative approach to improve the life of a solid-acid catalyst. To achieve it, a suitable carrier microstructure is a critical factor.<sup>7</sup>

The anion of HPA (heteropoly acid) is a kind of polyoxometallic cluster formed by corner-sharing and edge-sharing polyhedra. In essence, the clusters have high molecular symmetry, electron transfer and thermal stability.<sup>8</sup> HPA, acid

stronger than sulfate acid, is usually employed in the industrial process as homogeneous catalyst, such as esterification, hydration reaction, isomerization and rearrangement *etc.*<sup>9</sup> The heterogeneous HPA-type catalyst is mainly constructed by coupling with types of carriers such as carbon materials, zeolites, silica, zirconia, titania and so on.<sup>10</sup> However, the weak interaction between HPA and carrier is easily resulted in leaching of HPA from carriers, which largely impedes the industrial applications of heterogeneous catalyst of HPA-type.

In past two decades, a kind of porous material called as the MOF (metal–organic framework), analogous of zeolite in a simplified way, has been flourishing owing to extensive applications in the fields of gas-separation/gas-storage, drug delivery, chemical sensor and so forth.<sup>11–13</sup> The channel and cage of MOF microstructure are set up from the cation/cationic oxo-cluster as the node and bi-dentate/multi-dentate organic ligand as the linker.<sup>14,15</sup> Therefore, MOF materials with the designable and tunable channel or cage, high crystallinity, large surface area, extraordinarily thermal and chemical stability, especially are suitable for carrier.

It is apparently deduced that a novel approach to establish the heterogeneous catalyst of HPA-type is to encapsulate the HPA into the designable and tunable channel or cage of MOF.<sup>16</sup> Even early, G. Ferey *et al.* have accomplished to load the heteropoly acid into MIL-101 super-cage when they synthesized the

School of Chemical Engineering, Changchun University of Technology, 130012, Changchun, P. R. China. E-mail: [wyr@ccut.edu.cn](mailto:wyr@ccut.edu.cn); [liyafeng@ccut.edu.cn](mailto:liyafeng@ccut.edu.cn); Fax: +86-0431-85716785



MIL-101.<sup>17</sup> Afterwards, HPA@MOF composites have continuously been reported on the basis of the MOF type, such as KKUST-1,<sup>18</sup> MIL-101,<sup>19</sup> IRNENU,<sup>20</sup> HKUST-1(MOF-199),<sup>21,22</sup> MIL-100,<sup>23</sup> MIL-53,<sup>24</sup> ZIF-8,<sup>25,26</sup> NU-1000,<sup>27,28</sup> UIO-66 (ref. 29 and 30) and so forth. Among them, UIO-66 and analogies which are formed by the  $Zr_6(OH)_4O_4(CO_2)_{12}$  cluster as the node, have drawn more attentions due to the extraordinarily chemical and thermal stability.<sup>31</sup> Notably, UIO-66 is able to steadily exist for several months in pH = 1–11 of the water.<sup>32</sup> UIO-66 simplified to fcu-type zeolite bears the tetrahedral and octahedral cages (0.74 nm/0.84 nm) in typical structure.<sup>33</sup> Normally, both cages are incapable of accommodating the ~1 nm typical Keggin-type HPA molecule. The loaded HPA would distribute the outer surface of UIO-66 or be embedded into the interior of UIO-66 by ruining the UIO-66 framework. The consecutive researches show that the modulated agent like mono-carboxylic acid can sufficiently promote the cage size by reducing the ligand numbers of  $Zr_6(OH)_4O_4(CO_2)_{12-x}$  ( $x = 1, 2$ ).<sup>34,35</sup> Therefore, the enlarged cage of UIO-66 is theoretically big enough to accommodate the typical Keggin-type HPA molecule.

Biodiesel, representing a clean and sustainable energy source, is a promising alternative for fossil fuel-based energy systems.<sup>36,37</sup> The raw material—vegetable oil comprises of fatty glycerides and small amount of free fatty acids. The simultaneous transesterification and esterification can convert all of them into fatty acid methyl ester (FAME). The cooked vegetable oil would contain more free fatty acids owing to the hydrolysis during food processing. The cooked vegetable oil should strictly be pretreated because the strong base (KOH, NaOH) as catalyst would happen to saponify with free fatty acids in cooked vegetable oil. Therefore, the acid, especially solid acid, is a competent one. The zirconium-based metal–organic framework is a potential carrier to set up the solid acid of POM@MOF type owing to the designable and tunable cage structure and chemical and thermal stability. The direct assembly is a facile method to encapsulate HPA into the cage of UIO-66 without ruining the framework. Lately, Xie *et al.* have described one-pot transesterification-esterification of acidic vegetable oil over a functionalized AILs/POM/UIO-66-2COOH (AIL =  $[SO_3H-(CH_2)_3-HIM][HSO_4]$  ionic liquid; POM: Keggin- $H_3PW_{12}O_{40}$ ).<sup>38</sup> Notably, the AILs/POM/UIO-66-2COOH composite can combine the advantages of AIL, POM and Zr-MOF to present the good catalytic performance. However, with either UiO-66-2COOH or POM/UIO-66-2COOH as the catalyst, the conversions of soybean oil are low. Under circumstance of POM/UIO-66-2COOH, the conversion of soybean oil is just over 30%. The other works like NiHSIW/UIO-66 (ref. 39) and ZrSIW/UIO-66 (ref. 40) shows that POM@UIO-66 is only capable of catalyzing the esterification of oleic acid. In our previous work, Keggin- $H_3PW_{12}O_{40}$  has directly been assembled into the cage of UIO-66 at a relatively high reaction temperature in the present of modulated agent.<sup>41</sup> However, the Keggin- $PW_{12}@UIO-66$  composite has failed to catalyze the transesterification of soybean oil into biodiesel.

Keggin- $PW_{12}@UIO-66$  is capable to catalyze the transesterification of soybean oil in some sense, so it needs to enhance the catalytic activity of Keggin- $PW_{12}@UIO-66$ . The synthesis always plays an important role in the synthesis–

structure–property relation. Kickelbick *et al.* describe the formation of  $Zr_6(OH)_4O_4(OMc)_{12}$  (OMc = methacrylate) by method of sol–gel at room temperature.<sup>42</sup> Furthermore, Guilmert *et al.* have utilized  $Zr_6(OH)_4O_4(OMc)_{12}$  (OMc = methacrylate) obtained at room temperature as the source of  $Zr_6(OH)_4O_4(CO_2)_{12}$  cluster, and then exchange OMc with terephthalic or *trans,trans*-muconic acids, to synthesize the UIO-66 and analogy from room temperature to 150 °C.<sup>43</sup> Conversely, DeStefano *et al.* have prepared the  $Zr_6(OH)_4O_4(Ac)_{12}$  (HAc = acetic acid) at high temperature with a present of acetic acid and then exchanged the HAc with terephthalic at room temperature.<sup>44</sup> Accordingly, in present work, two-step method—high-temperature formation of  $Zr_6(OH)_4O_4(Ac)_{12}$  and low-temperature self-assembly of  $PW_{12}@UIO-66$ , has tentatively been adopted to prepare  $PW_{12}@UIO-66$  composite. At first step,  $Zr_6(OH)_4O_4(Ac)_{12}$  is formed at high temperature in a present of acetic acid. At second step, the reaction temperature has been lowered to prepare  $PW_{12}@UIO-66$  composite. Furthermore, as-synthesized  $PW_{12}@UIO-66$  composite has been employed to convert the soybean oil to biodiesel.

## 2. Experimental sections

The edible soybean oil was purchased from a local Walmart (Changchun, China).  $ZrCl_4$  (zirconium(iv) chloride, >99%), HAC (acetic acid, >99%), DMF (*N,N*-dimethylformamide), BDC (1,4-benzenedicarboxylic acid, >99%),  $H_3PW_{12}O_{40} \cdot xH_2O$  (12-tungstophosphoric acid, >99%), methanol (>99%), provide by Aladdin Co. (Shanghai, China). All other chemicals were obtained commercially and used as received.

The  $PW_{12}@UIO-66$  composite was solvothermally synthesized by the method of two steps—high-temperature preparation of  $Zr_6O_4(OH)_4(CH_3COO)_{12}$  and low-temperature self-assembly of  $PW_{12}@UIO-66$  composite.<sup>44</sup> Typically,  $ZrCl_4$  (0.75 g, 3.22 mmol) was dissolved into mixed solution of acetic acid (25 ml, 436.8 mmol)/DMF (200 ml, 2.4 mol) to clear solution and continuously stirred for half an hour. The mixture was heated up to 130 °C for 4 hours in the oven. Then, the solution was cooled down to 70 °C. BDC (0.6 g, 3.613 mmol) and  $H_3PW_{12}O_{40} \cdot xH_2O$  (40 mg) were successively dissolved into the solution at 70 °C. Finally, the clear solution was still crystallized in 70 °C of the oven for 48 hours. After naturally cooled to room temperature, the product was centrifugally separated at 5000 rpm for 5 min, washed and centrifuged three times using methanol. The as-synthesized product was dried at 70 °C overnight. The yield of  $PW_{12}@UIO-66$  composite was estimated about 95% based on UIO-66 ( $Zr_6O_4(OH)_4(BDC)_6$ ). The content of  $PW_{12}$  was 4.1%. The utilization of  $H_3PW_{12}O_{40}$  was 85%.

The reaction of soybean oil with methanol was carried out in a glass vial.<sup>38</sup> Concretely, 1 g of soybean oil was dissolved into mixed solution of 5.5 ml of methanol and 1.5 ml of THF (tetrahydrofuran) as phase transfer catalyst. Then, 200 mg of  $PW_{12}@UIO-66$  was added. The mixture was heat up to 75 °C and reacted for 4 h. After naturally cooled to room temperature, the catalyst was centrifugally separated at 5000 rpm for 5 min. The supernatant was condensed to remove the solvents at 70 °C. The

product was washed by water. The oil phase was the biodiesel. The water phase was vaporized to get the glycerol.

The recycling of  $\text{PW}_{12}@ \text{UIO}-66$  composite was investigated.<sup>45</sup> The separated  $\text{PW}_{12}@ \text{UIO}-66$  composite was simply washed and centrifuged using methanol, and naturally dried at ambient temperature. Then, it was recycled under an optimal condition. As for the life, since the performance of  $\text{PW}_{12}@ \text{UIO}-66$  composite was inquired, the reactant and product and  $\text{PW}_{12}@ \text{UIO}-66$  composite were together sealed in autoclave for two weeks, three weeks and four weeks, respectively. The  $\text{PW}_{12}@ \text{UIO}-66$  composite was weekly taken out, handled and characterized. The activity of  $\text{PW}_{12}@ \text{UIO}-66$  composite was carried out under an optimal condition.

Powder X-ray diffraction (PXRD) patterns were recorded on a Rigaku D/MAX PC2200 diffractometer for Cu  $K\alpha$  radiation ( $\lambda = 1.5406 \text{ \AA}$ ), with a scan speed of  $5^\circ \text{ min}^{-1}$ . Fourier transform infrared (FTIR) spectra were recorded within the  $400\text{--}4000 \text{ cm}^{-1}$  region on a Nicolet iS10 FTIR spectrometer using KBr pellets. The morphologies of the samples were inspected on a transmission electron microscope (TEM, JEOL-2000ex). The surface morphology and elemental composition were examined by transmission electron microscopy (TEM, JEM-2100F) and energy-dispersive X-ray (EDX) spectroscopy (Oxford Instruments X-MaxN 80T). The  $\text{PW}_{12}$  content was determined by IRIS Intrepid II ICP instrument (Thermo Electron Corp.). The  $\text{PW}_{12}@ \text{UIO}-66$  composite was dissolved by the piranha solution ( $\text{H}_2\text{SO}_4/\text{H}_2\text{O}_2$ ) and diluted to a certain concentration.  $\text{N}_2$  isothermal adsorption experiments were performed at 77 K with TriStar II 3020 (Micromeritics Instrument Corporation) apparatus using nitrogen as the probing gas. The samples were vacuumed for 10 h at  $120^\circ \text{C}$  before the data were collected. In context, all specific surface areas are referred to the BET (Brunauer–Emmett–Teller) specific surface area. The thermal gravimetric analyses (TG) were performed on Pyris STA 6000 instrument used in a nitrogen environment with a heating rate of  $10^\circ \text{C min}^{-1}$  and  $\text{N}_2$  flow of  $20 \text{ ml min}^{-1}$ . X-ray photoelectron spectrometry (XPS) data was acquired using an X-ray photoelectron spectrometer with monochromatic Al  $K\alpha$  X-ray (ESCALABMKLL, VG Co.). The conversion of biodiesel was quantified by the standard calibration on Agilent 1100 HPLC (Ultrasphaera ODS column:  $4.6 \text{ mm} \times 15 \text{ cm}$ ; mobile phase: acetonitrile : water = 15 : 85; rate of flow:  $1 \text{ ml min}^{-1}$ ; column temperature:  $40^\circ \text{C}$ ; ultra-violet wavelength of detector:  $210 \text{ nm}$ ).

### 3. Results and discussions

Ensuring the phase purity and crystallinity of active component and carrier is essentially important for designing and preparing the novel kind of catalyst. In our work,  $\text{PW}_{12}@ \text{UIO}-66$  composite is solvothermally implemented through two-step method. PXRD technique has been utilized to verify the phase purity and crystallinity of the products with contrast to simulated UIO-66 (Fig. 1). Comparably, the entire diffraction peaks of two as-synthesized products—UIO-66 and  $\text{PW}_{12}@ \text{UIO}-66$ , completely consist with those of simulated UIO-66, proving the phase purity of both products. Meanwhile, the sharp diffraction peak at (111) facet shows the crystallinity of the products. No XRD

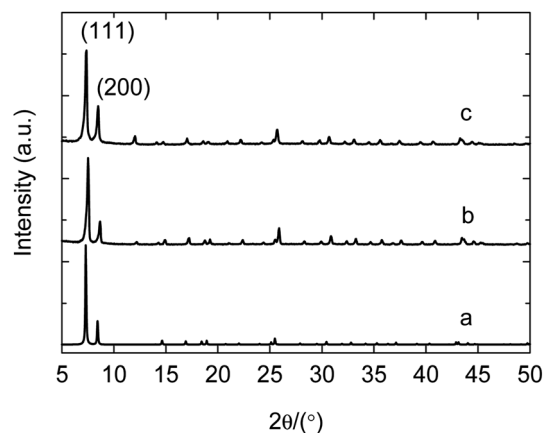


Fig. 1 PXRD patterns. (a) Simulated UIO-66 calculated from cif.file; (b) experimental UIO-66; (c) as-synthesized  $\text{PW}_{12}@ \text{UIO}-66$ .

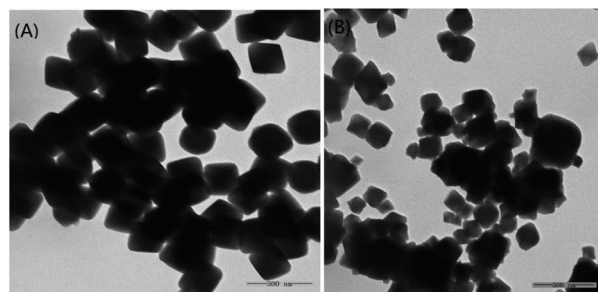


Fig. 2 TEM diagrams of UIO-66 (A) and  $\text{PW}_{12}@ \text{UIO}-66$  (B).

peaks corresponding to HPW are found, suggesting that the homogeneous dispersion of active components on the UIO-66 supports. Such XRD results imply that the primary crystallinity of UIO-66 structure is not obviously destroyed during the preparation processes of the solid catalyst, which would be beneficial for the heterogeneously catalytic transesterification.

With implantation of active component, the morphology of carrier in composite is easily ruined into pieces or transformed owing to the growth along with dominant facets. This may generate more active sites, but the life relatively becomes low due to the leaching of active component. Namely, the good morphology of composite, especially identical with that of carrier, may endow the robust structure and probable long life. The morphology of as-synthesized composite is inspected by TEM (Fig. 2). As seen from Fig. 2(A), UIO-66 as carrier shows the morphology of uniformed and integrated octahedron under this reaction condition, completely consisting with ref. 46. The as-synthesized  $\text{PW}_{12}@ \text{UIO}-66$  composite (Fig. 2(B)) also exhibits the identical morphology of octahedron like UIO-66, which represents the robust structure of composite. The robust structure of  $\text{PW}_{12}@ \text{UIO}-66$  composite could be helpful to improve life.

In  $\text{PW}_{12}@ \text{UIO}-66$  composites,  $\text{PW}_{12}$  is qualitatively measured by FTIR spectrum. The IR characteristic vibrations of  $\text{PW}_{12}$  involve  $1085 \text{ cm}^{-1}$  (P-Oa),  $964 \text{ cm}^{-1}$  (W-Od),  $870 \text{ cm}^{-1}$  (W-Ob-W), and  $804 \text{ cm}^{-1}$  (W-Oc-W).<sup>38</sup> However, as shown in Fig. 3,

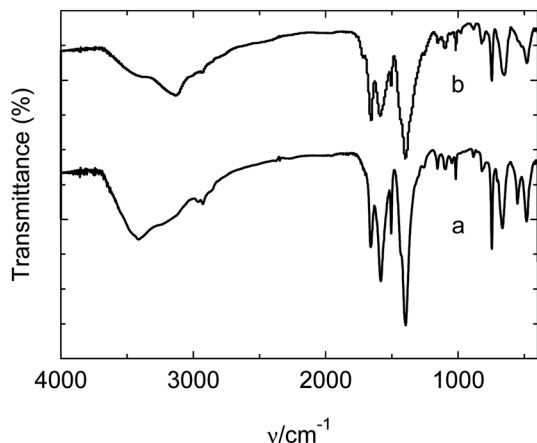


Fig. 3 FTIR curves. (a) UIO-66; (b)  $\text{PW}_{12}$ @UIO-66 composite.

the characteristic vibrations are too weak to be distinguished. Furthermore, elemental analysis of  $\text{PW}_{12}$ @UIO-66 composite is qualitatively examined by energy-dispersive X-ray (EDX) spectroscopy (Fig. 4(A)–(E)), suggesting the existence of  $\text{PW}_{12}$ @UIO-66 composite. The W and P elements are well-distributed in UIO-66, which is consistent with results of PXRD. The quantitative analysis of  $\text{PW}_{12}$  is implemented by IRIS Intrepid II ICP instrument. The content of  $\text{PW}_{12}$  in  $\text{PW}_{12}$ @UIO-66 composite is about 4.1%, and at meantime the utilization of  $\text{H}_3\text{PW}_{12}\text{O}_{40}$  is beyond 85%. The W valence state in  $\text{H}_3\text{PW}_{12}\text{O}_{40}$  would be varied with reaction condition. Therefore, the valence state and composition of as-synthesized  $\text{PW}_{12}$ @UIO-66 composite are confirmed by X-ray photoelectron spectrometer (Fig. 5). The XPS spectra survey has showed the co-existence of W, P, Zr, C and O elements, clearly indicating the existence of  $\text{PW}_{12}$ @UIO-66 composite (Fig. 5(A)). The W fitting peaks of binding energy locate 36.9 eV and 34.8 eV, which are attributed to the  $\text{W}^{5+} 4f_{5/2}$

and  $\text{W}^{5+} 4f_{7/2}$ . This means that the most of  $\text{W}^{6+}$  of  $\text{PW}_{12}$  in UIO-66 is reduced to  $\text{W}^{5+}$  under this reaction condition (Fig. 5(B)).

Based on the reaction kinetics theory of heterogeneous catalysis, high specific surface area can speed up reaction rate. The theoretically calculated specific surface area and cage size of UIO-66 is  $954 \text{ m}^2 \text{ g}^{-1}$  and 0.74 nm (tetrahedron cage)/0.86 nm (octahedron cage), respectively. With adding modulated agent, the ligand may gradually be lost and simultaneously the specific surface area and porous size are correspondingly enlarged. It is convinced that specific surface area can achieve  $1433 \text{ m}^2 \text{ g}^{-1}$  with loss of one BDC and  $1967 \text{ m}^2 \text{ g}^{-1}$  with loss of two BDC.<sup>34,35</sup> In general, specific surface area of loaded carrier is less than that of carrier itself. At the highly synthetic temperature such as  $120^\circ \text{C}$ , specific surface area of  $\text{PW}_{12}$ @UIO-66 obeys this rule. The specific surface area of UIO-66 and  $\text{PW}_{12}$ @UIO-66 prepared at  $120^\circ \text{C}$  are  $1382 \text{ m}^2 \text{ g}^{-1}$  and  $1268 \text{ m}^2 \text{ g}^{-1}$  (Fig. 6(A)), respectively. In this work, specific surface area of UIO-66 prepared at  $70^\circ \text{C}$  is up to  $1387 \text{ m}^2 \text{ g}^{-1}$ , which basically is the same as one at  $120^\circ \text{C}$ . However, when  $\text{H}_3\text{PW}_{12}\text{O}_{40}$  is introduced into the reaction system, specific surface area of  $\text{PW}_{12}$ @UIO-66 dramatically increases up to  $1960 \text{ m}^2 \text{ g}^{-1}$ . As seen in Fig. 6(B), the remarkable difference between UIO-66 and  $\text{PW}_{12}$ @UIO-66 is that adsorption–desorption curve of  $\text{PW}_{12}$ @UIO-66 exists a bigger hysteresis loop. The hysteresis loop is usually denoted as the formed mesopores. According to ref. 34 and 35, the ligand loss may improve the specific surface area of UIO-66 and expand the pore size. Under relatively high temperature ( $120^\circ \text{C}$ ), the linkage between  $\text{Zr}_6\text{O}_4(\text{OH})_4$  cluster and BDC is thermodynamically strong. The  $\text{PW}_{12}$  is only encapsulated in UIO-66 as the specific surface area of  $\text{PW}_{12}$ @UIO-66 decreases. With decreasing the temperature, the linkage between  $\text{Zr}_6\text{O}_4(\text{OH})_4$  cluster and BDC becomes weak owing to the prolong of reaction time.<sup>44</sup> It is speculated that  $\text{PW}_{12}$  molecule may not only be encapsulated in UIO-66 but also act as the modulated agent to improve the specific surface area and expand the pore size by

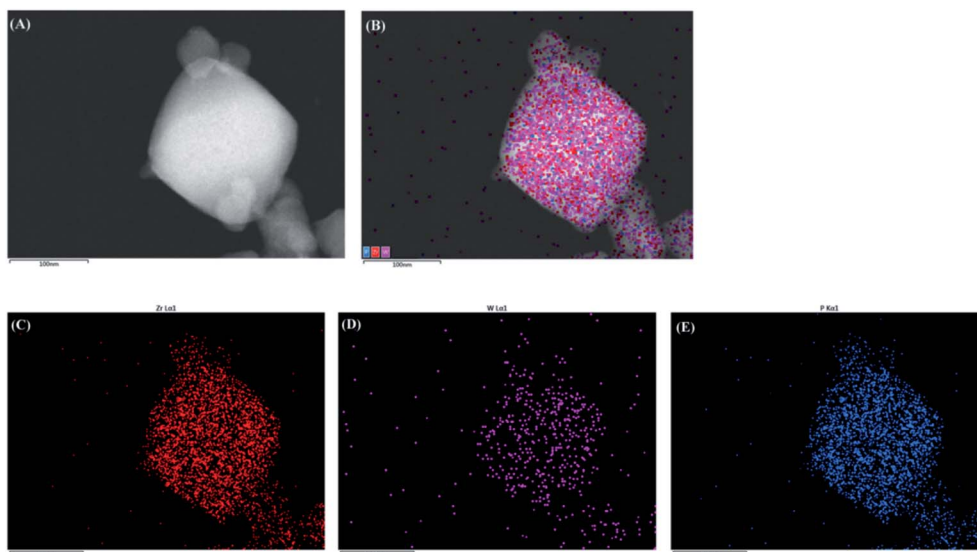


Fig. 4 TEM and the corresponding STEM image of (A)  $\text{PW}_{12}$ @UIO-66 composite and the corresponding elemental mappings of (B) all elements, (C) Zr, (D) W and (E) P.



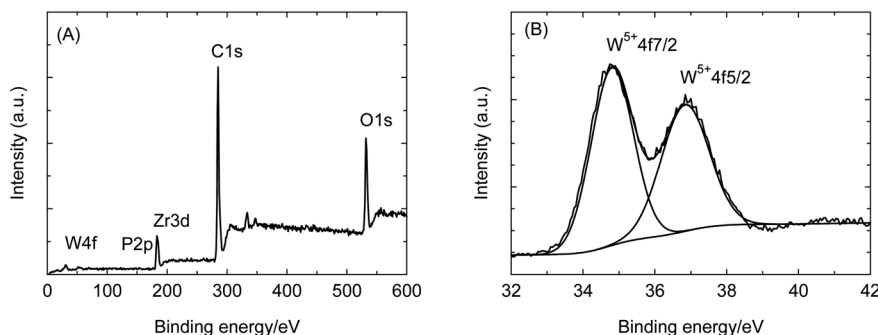


Fig. 5 XPS spectra of  $\text{PW}_{12}@UIO-66$  composite. (A) Survey; (B) the fitting peak of W 4f.

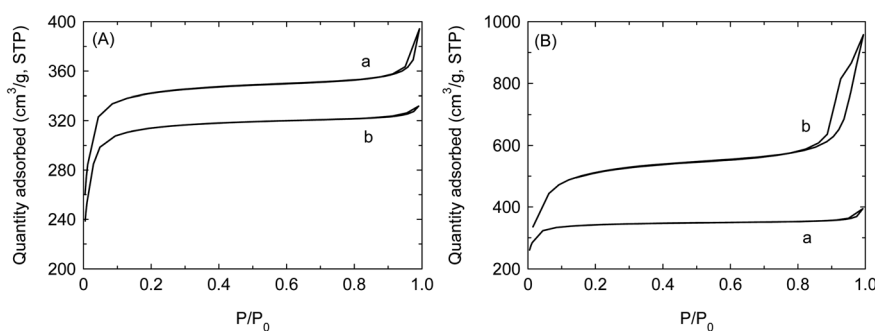


Fig. 6  $\text{N}_2$  isothermal adsorption at 77 K. (A) Reaction temperature: 120 °C. (a) SSA (specific surface area) of UIO-66:  $1382 \text{ m}^2 \text{ g}^{-1}$ ; (b) SSA of  $\text{PW}_{12}@UIO-66$  composite:  $1268 \text{ m}^2 \text{ g}^{-1}$ . (B) Reaction temperature: 70 °C. (a) SSA of UIO-66:  $1387 \text{ m}^2 \text{ g}^{-1}$ ; (b) SSA of  $\text{PW}_{12}@UIO-66$  composite:  $1960 \text{ m}^2 \text{ g}^{-1}$ .

reducing the BDC. At meantime, this means that  $\text{PW}_{12}$  is well-distributed in UIO-66. The formed mesopores apparently would allow bigger molecule to penetrate the channel and cage of  $\text{PW}_{12}@UIO-66$  composite.

The thermal stability of catalyst is an important feature, which can be allowed to endure the local hotspot of exothermic reaction. Thus, it is helpful to improve the quality of product and prolong the life of catalyst. As shown in Fig. 7, decomposed temperature of UIO-66 is coincided with the ref. 31 about 500 °C, indicating that the preparation condition in this work hardly affects the thermal stability of UIO-66. As for  $\text{PW}_{12}@UIO-$

66 composite, there is a sharp weight loss from 500 °C to 600 °C, which is belonged to the decomposition of UIO-66. This shows that the thermal stability of  $\text{PW}_{12}@UIO-66$  maintain unchanged in spite of encapsulating  $\text{PW}_{12}$ . The weight loss below 250 °C is assigned to crystal water and structure water and solvent of  $\text{PW}_{12}$ . The decomposed temperature of  $\text{PW}_{12}$  is about 470 °C. However, the content of  $\text{PW}_{12}$  is relatively low and the weight loss mainly results from phosphor. Thus, the weight loss of  $\text{PW}_{12}$  is not observed.

The  $\text{PW}_{12}@UIO-66$  composite is synthesized by two steps, high-temperature preparation of  $\text{Zr}_6\text{O}_4(\text{OH})_4(\text{CH}_3\text{COO})_{12}$  and low-temperature self-assembly of  $\text{PW}_{12}@UIO-66$ . The synthetic procedure and main results simultaneously are illustrated as in Scheme 1. It can be concluded that this route gives rise to high utilization of active component and high yield, and as-synthesized  $\text{PW}_{12}@UIO-66$  composite exhibits robust structure and big specific surface area and high thermal stability. Accordingly, catalysis of  $\text{PW}_{12}@UIO-66$  composite is further investigated.

The biodiesel (fatty acid methyl ester, FAME) is theoretically manufactured by the simultaneous transesterification and esterification of plant oil or cooking one since the raw material comprises of fatty glycerides and small amount of free fatty acids. In present, the industrial process with strong base (KOH) as the catalyst has been becoming the mainstream. However, the process is complicated as the raw material must be refined to avoid the saponification caused by free fatty acid and on the

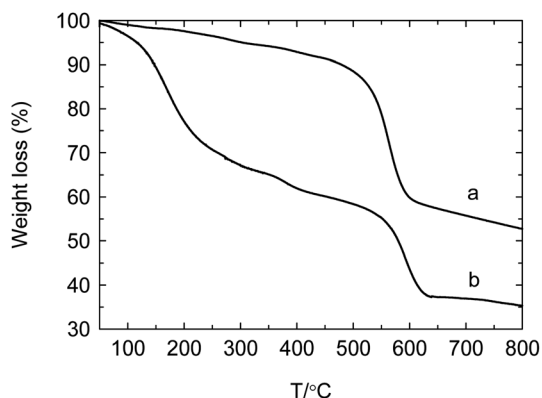
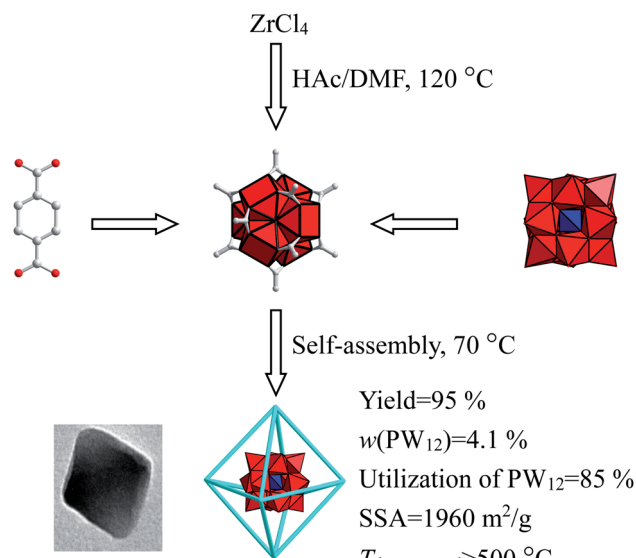
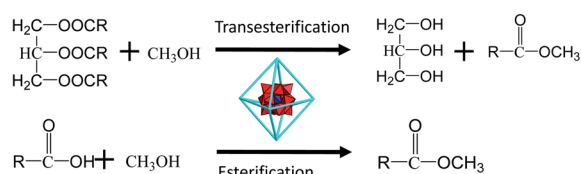


Fig. 7 TG curves. (a) UIO-66; (b)  $\text{PW}_{12}@UIO-66$  composite.



Scheme 1 Synthetic procedure of  $PW_{12}@UIO-66$  composite and main results.



Scheme 2 Simultaneous transesterification and esterification of soybean oil into biodiesel.

other hand the used base catalyst is necessarily recalled with respect to environmental problem. The mineral acid can catalyze both transesterification and esterification, and then the raw material is not necessarily refined and the operation is correspondingly simply. However, acid corrosion to the apparatus is very serious and the acid is necessarily recalled as well. The solid acid is one of a promising candidate for environmental benign, non-corrosion, easy separation and recycling. However, the catalyst life seriously restrains the industrial application of the solid acids. Since HPA (heteropoly acid) can be loaded on MOF, HPA@MOF composite is endowed as the feature of solid acid. Zhang *et al.* suggest that esterification of oleic acid is implemented by HPA@MOF composite as acidic center to activate the carbonyl group of oleic acid and generate the  $C^+$  ion which is attacked by methanol.<sup>45</sup> In this work, with soybean oil (fatty glycerides and small amount of free fatty acids) as raw material, the transesterification is accomplished by  $PW_{12}@UIO-66$  composite as acid center to activate the carbonyl and replace the glycerol with methanol. The concisely synthetic route is illustrated in Scheme 2.

The soybean oil comprises of fatty glyceride and little free fatty acid. The methanol serves as both reactant and solvent. The free fatty acid is soluble in methanol, and at meantime the fatty glyceride is sparingly soluble in methanol. Raising the

temperature or methanol/oil ratio can enhance the solubility of fatty glyceride. However, the volatile and flammable methanol is not safe in high temperature, which generates more cost of the apparatus and complicated operation. To raise the solubility of fatty glyceride, THF is introduced as phase transfer catalyst to improve the miscibility of fatty glyceride and methanol. Besides, the present industrial process with KOH as catalyst adopts moderate reaction temperature.

The effects on the conversion of soybean oil into biodiesel involves in catalyst amount, solvent amount, reaction time, reaction temperature and phase transfer catalyst. The single factor including catalyst amount, methanol amount, reaction temperature, reaction time and phase transfer catalyst, is successively implemented with fixing the rest variables. The amount of  $PW_{12}@UIO-66$  composite is correlated with active sites. With increasing the amount of  $PW_{12}@UIO-66$  composite, the conversion of soybean oil sharply rises (Fig. 8(A)). After 200 mg of  $PW_{12}@UIO-66$  composite is added, the conversion rises slowly. Although the high ratio of methanol/soybean oil can promote the process, more methanol means more cost (Fig. 8(B)). After 5.5 ml of methanol is employed, the conversion rises flatly. Both transesterification and esterification are the kinetic equilibrium. After 4 h, the conversion basically remains constant (Fig. 8(C)). The high reaction temperature can improve the activity of  $PW_{12}@UIO-66$  composite, but the high reaction temperature would bring out the energy consumption and safety problem owing the volatile and flammable methanol. After 75 °C of reaction temperature, the conversion rises flatly (Fig. 8(D)). The THF as phase transfer catalyst can boost the miscibility of methanol and soybean oil under low temperature. Till 1.5 ml THF, the conversion exceeds 90% (Fig. 8(E)). Under the optimal reaction conditions, 200 mg of  $PW_{12}@UIO-66$  composite as catalyst, 5.5 ml of methanol and 1.5 ml of THF as the phase transfer catalyst vs. 1 g of soybean oil, 4 h of reaction time and 75 °C of reaction temperature, the conversion of soybean oil is beyond 90%. The soybean oil, catalyst ( $PW_{12}@UIO-66$  composite) and products (biodiesel and glycerol) are illustrated in Fig. 8(F).

The millions of tons of the cooked vegetable oil are generated every year.<sup>47</sup> The hugely economic value has been drawing the increasing attentions. The fatty glyceride of vegetable oil is hydrolyzed into the free fatty acid under the high temperature and water of food processing. So, the cooked vegetable oil contains the much free fatty acid. Additionally, the cooked vegetable oil can generate the toxic polycyclic aromatic hydrocarbons which is hardly edible. The cooked vegetable oil has further been simulated by mixing the soybean oil and the oleic acid to explore the conversion of biodiesel.  $PW_{12}$  as homogeneous catalyst is able to catalyze the simultaneous esterification and transesterification. However, the as-synthesized  $PW_{12}@UIO-66$  composite can catalyze the esterification and partial transesterification.<sup>38,41,45</sup> In the case of  $PW_{12}@UIO-66-2COOH$ ,<sup>45</sup> the efficiency of transesterification is just over 30%. In present work, the results show that the specific surface area of as-synthesized  $PW_{12}@UIO-66$  composite is substantially improved up to 1960  $m^2 g^{-1}$  and at meanwhile mesopores are formed. The improvement of specific surface area and

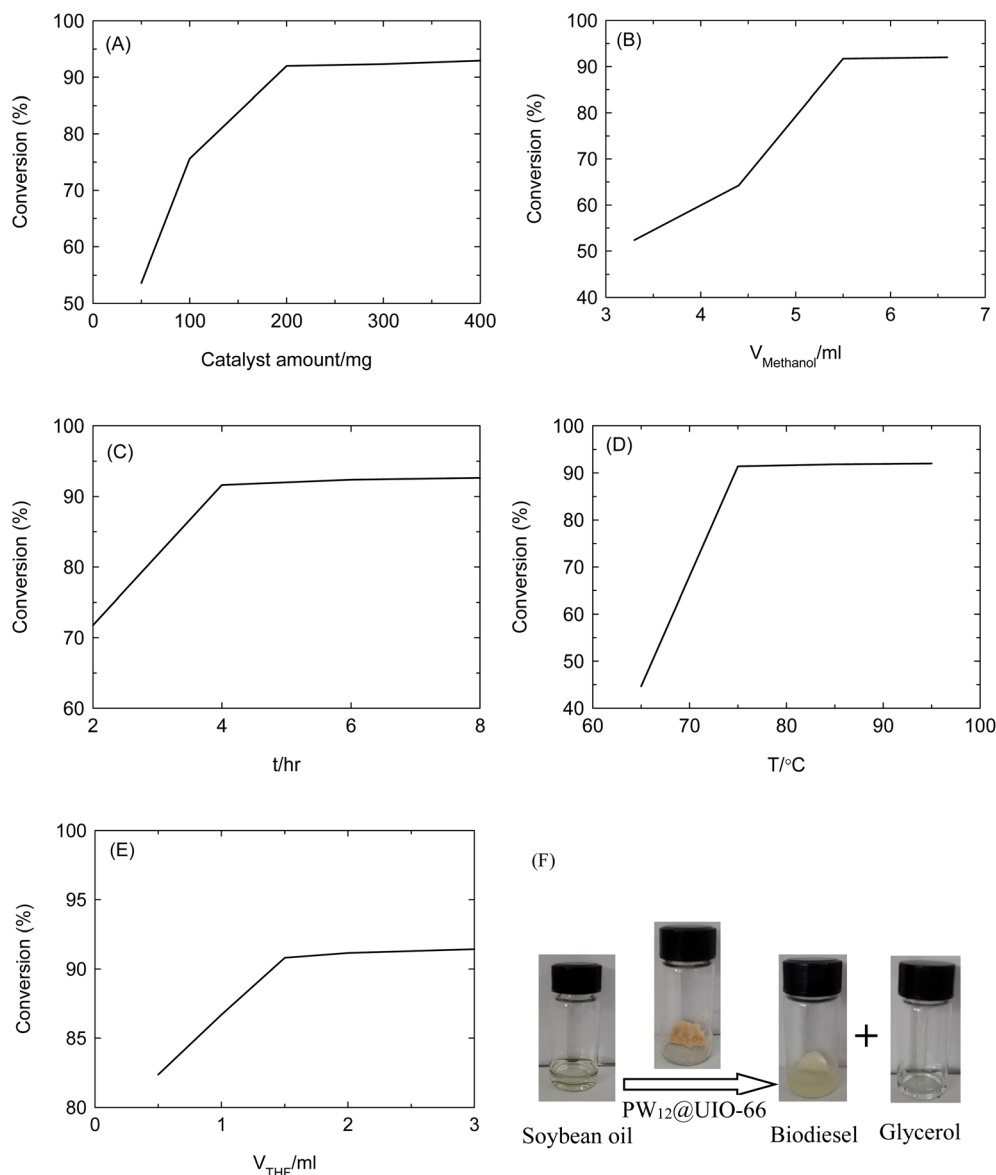


**Fig. 8** The effect of reaction conditions on the conversion of soybean oil and the yield of biodiesel by fixing the rest variables. The optimal reaction condition: 200 mg of  $\text{PW}_{12}@UIO-66$  composite, 5.5 ml of methanol and 1.5 ml of THF vs. 1 g of soybean oil, 4 h of reaction time and 75 °C of reaction temperature. (A) Catalyst amount; (B) methanol volume; (C) reaction time; (D) reaction temperature; (E) THF volume. (F) Illustrated procedure and production.

formation of mesopores are correlated with the number of lost BDC.<sup>34,35</sup> Then, the fatty glycerides can be allowed to diffuse into the enlarged channel and cage of  $\text{PW}_{12}@UIO-66$  composite and reacted to methanol over  $\text{PW}_{12}$  as acid center. The results show that  $\text{PW}_{12}@UIO-66$  composite has high activity to catalyze the simultaneous transesterification and esterification (Table 1).

The solid acid has the advantages including easy separation, non-corrosion and recycling, but the life is essentially fatal for the industrial application. Typical  $\text{SO}_4^{2+}/\text{ZrO}_2$  solid acid often loses the activity after 100–200 h at most. Enhancing the stability and prolonging the life are the crucial factors for the industrial prospect of solid acid. In the above work, the as-synthesized  $\text{PW}_{12}@UIO-66$  composite has displayed the high activity to catalyze the simultaneous transesterification and

esterification. The recycling experiment is implemented to verify the stability of  $\text{PW}_{12}@UIO-66$  composite. As shown in Fig. 9, the catalytic activity of  $\text{PW}_{12}@UIO-66$  composite basically

**Table 1** The result of the soybean oil, oleic acid and simulated acidic soybean oil catalyzed by  $\text{PW}_{12}@UIO-66$  composite<sup>a</sup>

Raw material	Amount	Conversion (%)
Soybean oil	1 g	91.1
Oleic acid	1 g	92.4
Soybean oil + oleic acid	0.9 g + 0.1 g	90.3

<sup>a</sup> The reaction condition: 200 mg of  $\text{PW}_{12}@UIO-66$  composite, 5.5 ml of methanol and 1.5 ml of THF, 4 h of reaction time and 75 °C of reaction temperature.

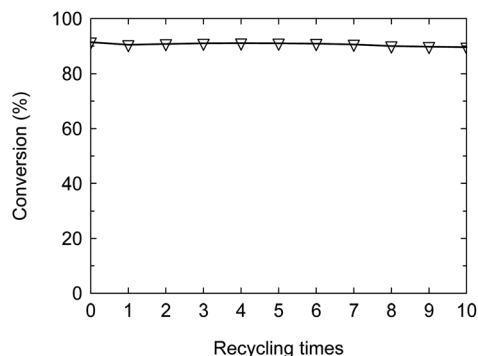


Fig. 9 The catalytic activity of  $\text{PW}_{12}@UIO-66$  composite after 10 times of recycling.

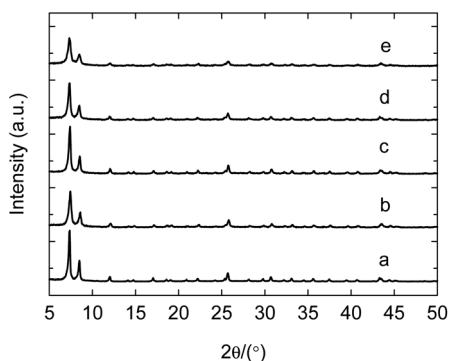


Fig. 10 PXRD patterns of used  $\text{PW}_{12}@UIO-66$  composite. (a) As-synthesized  $\text{PW}_{12}@UIO-66$  composite; (b) recycling 10 times; (c) 2nd week; (d) 3rd week; (e) 4th week.

remains unchanged after 10 cycles. At meanwhile, the used  $\text{PW}_{12}@UIO-66$  composite has been characterized by PXRD, TEM,  $\text{N}_2$  isothermal adsorption at 77 K and TG. PXRD shows that the used  $\text{PW}_{12}@UIO-66$  composite (Fig. 10b) is completely identical with the as-synthesized  $\text{PW}_{12}@UIO-66$  composite (Fig. 10a). The peak of the used  $\text{PW}_{12}@UIO-66$  composite is lightly broadened, probably owing to the slight framework deformation of UIO-66 caused by some reactants and productions. The morphology of the used  $\text{PW}_{12}@UIO-66$  composite maintains the shape of octahedron rather than debris, implying the robust framework (Fig. 11(A)). The BET specific surface area after 10 runs sharply declines due to the residue of the little reactants and products inside framework (Fig. 12a). The thermal stability of the used  $\text{PW}_{12}@UIO-66$  composite remains unchanged. These results testify the stability of  $\text{PW}_{12}@UIO-66$  composite (Fig. 13a).

To further explore the life of  $\text{PW}_{12}@UIO-66$  composite, the soybean oil, methanol, THF and  $\text{PW}_{12}@UIO-66$  composite has sealed into autoclave and kept the reaction temperature at 75 °C. The autoclave is sequentially taken out at 2<sup>nd</sup>, 3<sup>rd</sup> and 4<sup>th</sup> week. After simply treated, the used  $\text{PW}_{12}@UIO-66$  composite has also been characterized by PXRD, TEM,  $\text{N}_2$  isothermal adsorption at 77 K and TG. After four weeks, PXRD shows that the used  $\text{PW}_{12}@UIO-66$  composite is completely identical with

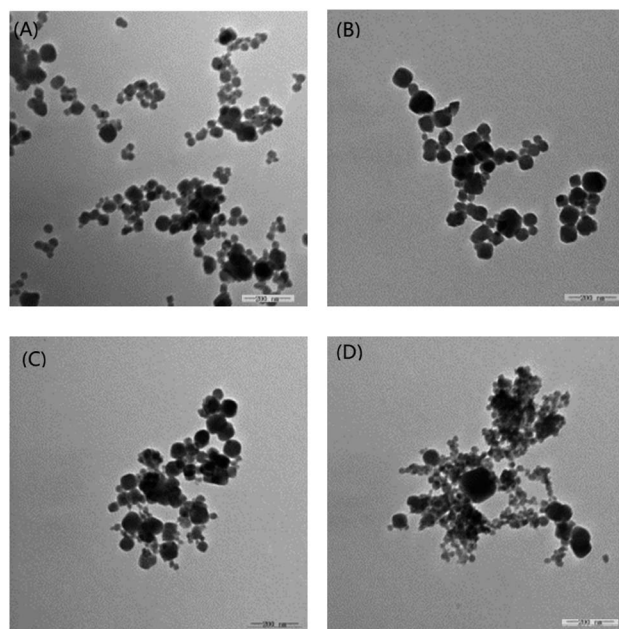


Fig. 11 TEM diagrams of used  $\text{PW}_{12}@UIO-66$  composite. (A) Recycling 10 times; (B) 2nd week; (C) 3rd week; (D) 4th week.

the as-synthesized  $\text{PW}_{12}@UIO-66$  composite (Fig. 10c–e). The peaks of the used  $\text{PW}_{12}@UIO-66$  composite are increasingly broadened, probably owing to the more framework deformations of UIO-66. The morphologies of the used  $\text{PW}_{12}@UIO-66$  composite still maintain the shape of octahedron (Fig. 11(B)–(D)). The specific surface areas gradually decline (Fig. 12b–d). The thermal stability of the used  $\text{PW}_{12}@UIO-66$  composite remains unchanged (Fig. 13b–d). According to the above reaction condition, the 4<sup>th</sup>-week  $\text{PW}_{12}@UIO-66$  composite is further employed to catalyze the transesterification of soybean oil. The results show that it still maintains highly catalytic activity and the conversion can reach up to 89.1%. Through four-week life experiment, the results show that  $\text{PW}_{12}@UIO-66$  composite still maintain the structural stability, good morphology, high specific surface area, thermal stability and catalytic activity.

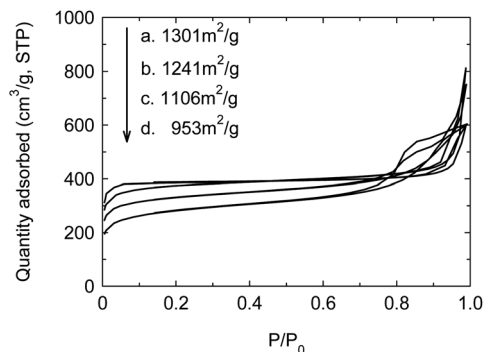


Fig. 12  $\text{N}_2$  isothermal adsorptions of used  $\text{PW}_{12}@UIO-66$  composite at 77 K. (a) Recycling 10 times; (b) 2nd week; (c) 3rd week; (d) 4th week.



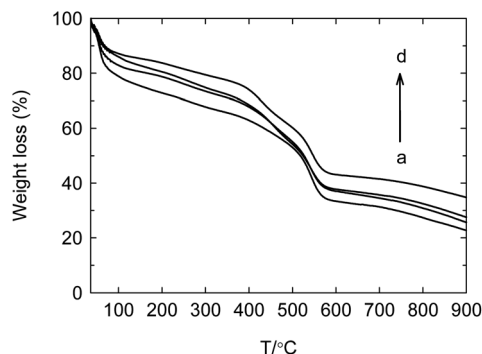


Fig. 13 TG curves of used PW<sub>12</sub>@UIO-66 composite. (a) Recycling 10 times; (b) 2nd week; (c) 3rd week; (d) 4th week.

## 4. Conclusion

In this work, PW<sub>12</sub>@UIO-66 composite synthesized by the method of two steps—high-temperature preparation of Zr<sub>6</sub>O<sub>4</sub>(-OH)<sub>4</sub>(CH<sub>3</sub>COO)<sub>12</sub> and low-temperature self-assembly of PW<sub>12</sub>@UIO-66 composite, shows good qualities as solid acid including high crystallinity, good octahedron morphology, big specific surface area and high thermal stability. Besides, this route gives rise to 95% yield and 85% utilization of H<sub>3</sub>PW<sub>12</sub>O<sub>40</sub>. The conversion of the soybean oil into biodiesel can exceed 90% under the optimal condition. The recycling and life experiments show that the structure and performance of PW<sub>12</sub>@UIO-66 composite after 10 times of recycling and 4 weeks maintain unchanged and at meantime PW<sub>12</sub>@UIO-66 composite still maintains high activity to convert the soybean oil into biodiesel.

## Conflicts of interest

There are no conflicts of interest to declare.

## Acknowledgements

This project was supported by Jilin Provincial Development and Reform Commission (No. 2019C043-1) and Jilin Provincial Education Department (No. JJKH20191298KJ).

## References

- S. Wang and G. Yang, *Chem. Rev.*, 2015, **115**, 4893–4962.
- M. E. Borges and L. Diaz, *Renewable Sustainable Energy Rev.*, 2012, **16**, 2839–2849.
- A. F. Lee, J. A. Bennett, J. C. Manayil and K. Wilson, *Chem. Soc. Rev.*, 2014, **43**, 7887–7916.
- T. Yamaguchi, *Catal. Today*, 1994, **20**, 199–217.
- K. Tanabe and T. Yamaguchi, *Catal. Today*, 1994, **20**, 185–198.
- S. Liu, M. Zhu and M. Iqbal, *Catal. Surv. Asia*, 2020, **24**, 196–206.
- J. Shi, L. Zhang and Z. Cheng, *Catal. Surv. Asia*, 2021, **25**, 279–300.
- X. López, J. J. Carbó, C. Bo and J. M. Poblet, *Chem. Soc. Rev.*, 2012, **41**, 7537–7571.
- M. N. Timofeeva, *Appl. Catal., A*, 2003, **256**, 19–35.
- E. Rafiee and S. Eavani, *RSC Adv.*, 2016, **6**, 46433–46466.
- M. P. Suh, H. J. Park, T. K. Prasad and D. W. Lim, *Chem. Rev.*, 2012, **112**, 782–835.
- L. E. Kreno, K. Leong, O. K. Farha, M. Allendorf, R. P. Van Duyne and J. T. Hupp, *Chem. Rev.*, 2012, **112**, 1105–1125.
- P. Horcajada, R. Gref, T. Baati, P. K. Allan, G. Maurin, P. Couvreur, G. Férey, R. E. Morris and C. Serre, *Chem. Rev.*, 2012, **112**, 1232–1268.
- D. J. Tranchemontagne, J. L. Mendoza-Cortés, M. O’Keeffe and O. M. Yaghi, *Chem. Soc. Rev.*, 2009, **38**, 1257–1283.
- M. Li, D. Li, M. O’Keeffe and O. M. Yaghi, *Chem. Rev.*, 2014, **114**, 1343–1370.
- C. T. Buru and O. K. Farha, *ACS Appl. Mater. Interfaces*, 2020, **12**, 5345–5360.
- G. Férey, C. Mellot-Draznieks, C. Serre, F. Millange, J. Dutour, S. Surble and I. Margiolaki, *Science*, 2005, **309**, 2040–2042.
- C. Y. Sun, S. X. Liu, D. D. Liang, K. Z. Shao, Y. H. Ren and Z. M. Su, *J. Am. Chem. Soc.*, 2009, **131**, 1883–1888.
- N. V. Maksimchuk, K. A. Kovalenko, S. S. Arzumanov, Y. A. Chesalov, M. S. Melgunov, A. G. Stepanov, V. P. Fedin and O. A. Kholdeeva, *Inorg. Chem.*, 2010, **49**, 2920–2930.
- F. J. Ma, S. X. Liu, C. Y. Sun, D. D. Liang, G. J. Ren, F. Wei, Y. G. Chen and Z. M. Su, *J. Am. Chem. Soc.*, 2011, **133**, 4178–4181.
- Q. Y. Zhang, C. Y. Yue, L. F. Ao, D. D. Lei, D. Ling, D. Yang and Y. T. Zhang, *Energy Sources, Part A*, 2019, 1–12.
- K. N. Abedin and J. S. Hwa, *Fuel Process. Technol.*, 2012, **100**, 49–54.
- J. Juanalcaniz, M. G. Goesten, E. V. Ramosfernandez, J. Gascon and F. Kapteijn, *New J. Chem.*, 2012, **36**, 977–987.
- A. Nikseresht, A. Daniyali, M. Alimohammadi, A. Afzalnia and A. Mirzaie, *Ultrason. Sonochem.*, 2017, **37**, 203–207.
- R. S. Malkar and G. D. Yadav, *Appl. Catal., A*, 2018, **560**, 54–65.
- N. A. Khan, B. N. Bhadra and S. H. Jhung, *Chem. Eng. J.*, 2018, **334**, 2215–2221.
- S. Ahn, S. L. Nauert, C. T. Buru, M. Rimoldi, H. Choi, N. M. Schweitzer, J. T. Hupp, O. K. Farha and J. M. Notestein, *J. Am. Chem. Soc.*, 2018, **140**, 8535–8543.
- C. T. Buru, A. E. Plateroprats, D. G. Chica, M. G. Kanatzidis, K. W. Chapman and O. K. Farha, *J. Mater. Chem. A*, 2018, **6**, 7389–7394.
- X. M. Zhang, Z. H. Zhang, B. H. Zhang, X. F. Yang, X. Chang, Z. Zhou, D. H. Wang, M. H. Zhang and X. H. Bu, *Appl. Catal., B*, 2019, **256**, 117804–117813.
- L. Ullah, G. Y. Zhao, Z. C. Xu, H. Y. He, M. Usman and S. J. Zhang, *Sci. China: Chem.*, 2018, **61**, 402–411.
- J. H. Cavka, S. Jakobsen, U. Olsbye, N. Guillou, C. Lamberti, S. Bordiga and K. P. Lillerud, *J. Am. Chem. Soc.*, 2008, **130**, 13850–13851.
- J. B. DeCoste, G. W. Peterson, H. Jasuja, T. G. Glover, Y. G. Huang and K. S. Walton, *J. Mater. Chem. A*, 2013, **1**, 5642–5650.

- 33 H. Furukawa, F. Gándara, Y. B. Zhang, J. C. Jiang, W. L. Queen, M. R. Hudson and O. M. Yaghi, *J. Am. Chem. Soc.*, 2014, **136**, 4369–4381.
- 34 H. Wu, Y. S. Chua, V. Krungleviciute, M. Tyagi, P. Chen, T. Yildirim and W. Zhou, *J. Am. Chem. Soc.*, 2013, **135**, 10525–10532.
- 35 W. B. Liang, C. J. Coghlan, F. Ragon, M. Rubio-Martinez, C. J. Kepert, D. M. D'Alessandro and R. Babarao, *Dalton Trans.*, 2016, **45**, 4496–4500.
- 36 W. J. Cong, S. Nanda, H. Li, Z. Fang, A. K. Dalai and J. A. Kozinski, *Green Chem.*, 2021, **23**, 2595–2618.
- 37 J. Sun, S. Abednatanzi, P. Van Der Voort, Y. Y. Liu and K. Leus, *Catalysts*, 2020, **10**, 578–610.
- 38 W. Xie and F. Wan, *Chem. Eng. J.*, 2019, **365**, 40–50.
- 39 Q. Zhang, D. Ling, D. Lei, T. Deng, Y. Zhang and P. Ma, *Green Process. Synth.*, 2020, **9**, 131–138.
- 40 Q. Zhang, D. Lei, Q. Luo, J. Wang, T. Deng, Y. Zhang and P. Ma, *RSC Adv.*, 2020, **10**, 8766–8772.
- 41 J. Y. Zhu, Z. Wang, X. L. Song, B. Y. Zhao, Y. F. Li and Y. R. Wang, *Micro Nano Lett.*, 2021, **16**, 90–96.
- 42 G. Kickelbick and U. Schubert, *Chem. Ber.*, 1997, **130**, 473–477.
- 43 V. Guillerm, S. Gross, C. Serre, T. Devic, M. Bauer and G. Férey, *Chem. Commun.*, 2010, **46**, 767–769.
- 44 M. R. DeStefano, T. Islamoglu, S. J. Garibay, J. T. Hupp and O. K. Farha, *Chem. Mater.*, 2017, **29**, 1357–1361.
- 45 Q. Zhang, D. Lei, Q. Luo, J. Wang, T. Deng, Y. Zhang and P. Ma, *RSC Adv.*, 2020, **10**, 8766–8772.
- 46 A. Schaate, P. Roy, A. Godt, J. Lippke, F. Waltz, M. Wiebcke and P. Behrens, *Chem.–Eur. J.*, 2011, **17**, 6643–6651.
- 47 U. Jamil, A. H. Khoja, R. Liaquat, S. R. Naqvi, W. N. N. W. Omar and N. A. S. Amin, *Energy Convers. Manage.*, 2020, **215**, 112934–112947.